The Kinetic Energy on a Continental Shelf from Topographic Rossby Waves Generated off the Shelf

JOHN KROLL

Old Dominion University, Norfolk, VA 23508

(Manuscript received 20 January 1978, in final form 8 January 1979)

ABSTRACT

Over a deep barotropic ocean an isolated pressure cell, producing a wind stress curl, generates topographic Rossby waves which are incident on a continental shelf with a simple exponentially varying slope. It is shown that this energy appears as a distinct peak at low frequency on the energy spectrum on the shelf. A peak at 0.05 cycles per day (cpd) in the spectrum from data of Smith (1974) for the Oregon shelf is consistent with this effect. For the case where topography dominates the beta effect off the shelf, general equations are found to estimate the frequency and dominant wavelength of the energy peak. An interesting result of this analysis is that, for all parameters being equal, this frequency should be lower on an eastern shelf than a western shelf in the Northern Hemisphere due to the beta effect. The variation of the magnitude and frequency of this peak with the location on the shelf, the distance of the center of forcing from the shelf, and the scale of the pressure cell is then investigated for the Oregon shelf in particular.

1. Introduction

In a previous paper (Kroll and Niiler, 1976; hereafter referred to as I) the transmission and decay properties of topographic Rossby waves (T-R waves) incident on an idealized exponential shelf were investigated. Here we consider a realistic meteorological forcing over the deep ocean generating long-period (much greater than the inertial period) and long-wavelength [$\geq$O(100 km)] waves onto a continental shelf. The purpose of this study is to show that this energy, produced completely off the shelf, can have a magnitude and frequency such as to appear distinctively in the energy spectrum on the shelf. To obtain general quantitative results for all possible ranges of the parameters is difficult and not done here. However, the case where topography off the shelf dominates the beta effect is found to be fairly easy to analyze using asymptotic methods. Also the specific case of the Oregon shelf is accurately analyzed using numerical means.

2. The model and equations of motion

As in I we assume the motion on the β-plane is barotropic, nondivergent and sufficiently weak to neglect nonlinear effects. Also, we again assume that the topographic slope is uniform in the longshore direction with the depth increasing exponentially away from shore. The right-handed coordinate system is fixed in the topography with y parallel to and x normal to the isobaths with positive x directed away from shore. Thus, the Coriolis parameter is given by $f = f_0 + \beta_c y + \beta_s x$, where $\beta_c = \beta \cos\theta$ and $\beta_s = \beta \sin\theta$ with f_0 and β being the usual quantities and θ is the angle measured counterclockwise between x and the eastward vector.

The constant slope parameter is defined by $S = h'(x)/h(x)$, where $h(x)$ is the depth. Our model consists of two exponential slopes with S_s being the slope parameter representing the shelf, while $S_0 \ll S_s$ represents the slope off the shelf. At the shelf break we define $x = 0$, and the depth there is denoted by H_0 (see Fig. 4 of I).

We assume that the ocean off the shelf is forced by the wind while the shelf is not. The equations from I governing the motion on the shelf and off the shelf respectively are

$$\nabla^2\psi_{s_t} + \beta_c\psi_{s_x} - S_s\psi_{s_{xt}} + (fS_s - \beta_s)\psi_{sy} = 0 \quad (2.1a)$$

and

$$\nabla^2\psi_{0_t} + \beta_c\psi_{0_x} - S_0\psi_{0_{xt}} + (fS_0 - \beta_s)\psi_{0_y} = \tau_y^{(x)} - \tau_x^{(y)} + S_0\tau^{(y)}, \quad (2.1b)$$

where the velocity components in x and y in terms of the streamfunction ψ are given respectively by $hu = -\psi_y$ and $hv = \psi_x$, and $\tau^{(x)}$ and $\tau^{(y)}$ are the wind stress components. The quantity $S_0\tau^{(y)}$ can be realistically neglected off the shelf in comparison to the stress curl $(\tau_x^{(y)} - \tau_y^{(x)})$. [Typically the stress curl is O(10^{-7} dyn cm^{-3}) and $S_0\tau$ is O(10^{-9} dyn cm^{-3}).]

At the shelf break, $x = 0$, we require the continuity of u and v. All other boundaries are open, so that we have radiation conditions for $x = \pm\infty$.

0022-3670/79/040712-12$07.00

We are neglecting reflections from shore by assuming that, because of bottom friction, only the energy of the incident wave to a point on the shelf is important. This assumption is based on calculations of the decay of long period and wavelength T-R waves from I.

3. The solution for a point source

In I we showed that wave solutions of the form

$$\psi = A \exp\left[\left(\frac{-i\beta_c}{2\sigma} + \frac{S}{2}\right)x + i\mu x + ily - i\sigma t\right] \quad (3.1)$$

are approximate solutions to the homogeneous parts of (2.1), where σ is frequency, l is the longshore wavenumber and

$$\mu^2 = -l^2 - \frac{l}{\sigma}(Sf_0 - \beta_s) - \left(\frac{S}{2}\right)^2 + \left(\frac{\beta_c}{2\sigma}\right)^2. \quad (3.2)$$

Here we let the wind stress curl in (2.1a) be given by $\delta(x - x_0)\delta(y - y_0)e^{-i\sigma t}$, Dirac delta functions centered at (x_0,y_0) and sinusoidal in time. We then assume a solution of the form

$$\psi = \exp\left[\left(\frac{-i\beta_c}{2\sigma} + \frac{S}{2}\right)x\right]e^{-i\sigma t}\frac{1}{2\pi} \times \int_{-\infty}^{\infty}\hat{\phi}(x,l)e^{ily}dl, \quad (3.3)$$

where $\hat{\phi}$ is the Fourier transform in y. Letting f be constant in (2.1), we obtain the following equations for $\hat{\phi}$ on and off the shelf, respectively:

$$\hat{\phi}_{s_{xx}} + \mu_s^2\hat{\phi}_s = 0, \quad (3.4a)$$

$$\hat{\phi}_{0_{xx}} + \mu_0^2\hat{\phi}_0 = -(1/\sigma) \times \exp\left[\left(\frac{i\beta_c}{2\sigma} - \frac{S_0}{2}\right)x_0\right]e^{-ily_0}\delta(x - x_0), \quad (3.4b)$$

where μ_0^2 and μ_s^2 are found from (3.2) using S_0 and S_s, respectively.

Using the continuity conditions at $x = 0$ and the condition that no energy (i.e., group velocity) is coming from $x = \pm\infty$, the solution for the streamfunction on the shelf in terms of convenient dimensionless quantities can be shown to be

$$\psi_s = \frac{ie^{-i\sigma t}}{2\pi\sigma}\exp\left[\left(i\bar{\beta}_c - \frac{S_0}{R}\right)\bar{x}_0 - \left(i\bar{\beta}_c - \frac{\bar{S}_s}{R}\right)\bar{x}\right] \times \int_{-\infty}^{\infty}\frac{\exp\{-i\alpha[\xi(\bar{y} - \bar{y}_0) - \bar{\mu}_s\bar{x} + \bar{\mu}_0\bar{x}_0]}{(\bar{S}_s - \bar{S}_0)/R + i(\bar{\mu}_s - \bar{\mu}_0)}d\xi, \quad (3.5)$$

where $\bar{\mu}_{0,s}^2 = \xi^2 + 2\xi(\bar{S}_{0,s} - \bar{\beta}_s) + \bar{\beta}_c^2 - \bar{S}_{0,s}^2/R^2$ and $\alpha = R\gamma x'$. The new dimensionless quantities are given by $\xi = -l/R\gamma$, $\bar{y} = y/x'$, $\bar{y}_0 = y_0/x'$, $\bar{x} = x/x'$, $\bar{x}_0 = x_0/x'$, and $(\bar{S}_0,\bar{S}_s,\bar{\beta}_s,\bar{\beta}_c) = (1/2\gamma)(S_0,S_s,\beta_s/f_0,\beta_c/f_0)$ where $R = f_0/\sigma$, $\gamma = \frac{1}{2}[(S_0 - \beta_s/f_0)^2 + (\beta_c/f_0)^2]^{1/2}$, and x' is the distance from the shelf break to the center of the forcing which will be applied later.

We denote the branch points associated with $\bar{\mu}_0 = 0$ and $\bar{\mu}_s = 0$ as $\xi_{0\pm}$ and $\xi_{s\pm}$, respectively, and write

$$\bar{\mu}_{0,s} = [(\xi - \xi_{0,s+})(\xi_{0,s-} - \xi)]^{1/2}, \quad (3.6)$$

where

$$\xi_{0,s\pm} = (\bar{S}_{0,s} - \bar{\beta}_s) \pm [(\bar{S}_{s,0} - \bar{\beta}_s)^2 + \bar{\beta}_c^2 - \bar{S}_{0,s}^2/R^2]^{1/2}.$$

We note that $(\bar{S}_0 - \bar{\beta}_s)^2 + \bar{\beta}_c^2 = 1$, so we can write $\xi_{0\pm} = \bar{S}_0 - \bar{\beta}_s \pm (1 - \bar{S}_0^2/R^2)^{1/2}$. If $R < \bar{S}_0$, $\xi_{0\pm}$ are not real and there are no waves from the source. However, we are interested in long-period waves ($R \gg 1$), so that $\xi_{0\pm}$ are always real since $\bar{S}_0 \leqslant 1$. From now on we will assume $(S_0/R)^2 \ll 1$ implying that $\xi_{0\pm} \approx \bar{S}_0 - \bar{\beta}_s \pm 1$. The branch cuts must be such that the integrand of (3.5) decays for ξ increasing from $\xi_{0,s+}$ and decreasing from $\xi_{0,s-}$. So the branch cuts from $\xi_{s,0-}$ must start upward and those from $\xi_{0,s+}$ downward on the $z = \xi + i\eta$ plane.

For a realistic shelf we have $\bar{S}_s \gg |\bar{\beta}_c|, |\bar{\beta}_s|$. Hence the beta effect can be neglected from the shelf, but the $\bar{S}_s^2/R^2$ term can be significant and is retained in (3.6). So we have $\xi_{s\pm} \approx \bar{S}_s[1 \pm (1 - 1/R^2)]^{1/2}$ and hence for $R^2 \gg 1$,

$$\xi_{s+} \approx 2\bar{S}_s, \quad \xi_{s-} \approx \bar{S}_s/2R^2. \quad (3.7)$$

It can be shown that because $S_s > S_0$, we always have $\xi_{s+} > \xi_{0+}$ and $\xi_{s-} > \xi_{0-}$.

The integrand is oscillatory for values of ξ such that $\xi_{s-} < \xi < \xi_{0+}$ which corresponds to the wavenumber "window" for waves to penetrate onto the shelf. The integrand decays for all values of ξ outside of this interval. If we set $\xi_{s-} = \xi_{0+}$ we obtain a minimum value for R, $R_{\min} = (\bar{S}_s/2\xi_{0+})^{1/2}$, below which no wave can come onto the shelf. Assuming $\bar{S}_s \gg \bar{S}_0$, $|\bar{\beta}_s|$, $|\bar{\beta}_0|$, we have $\xi_{s+} \gg \xi_{0+}$ and the integrand will have essentially vanished before ξ ever reaches ξ_{s+}. Thus the ξ values of interest are such that $\xi \ll \xi_{s+}$, and we can simplify $\bar{\mu}_s$ in (3.6) to

$$\bar{\mu}_s \approx \sqrt{2\bar{S}_s}(\xi - \xi_s)^{1/2}, \quad (3.8)$$

where from now on $\xi_s = \xi_{s-}$. Also it can be shown that the branch from ξ_s can be bent to eliminate any possibility of a pole. In fact, if $\bar{S}_s > R\bar{\beta}_c$ a vertical cut from ξ_s will eliminate the possibility of a pole.

We can find properties of the solution without integrating (3.5). The stationary points of the integral can be found by setting the ξ derivative of the eiconal part to zero. This yields

$$\bar{y} - \bar{y}_0 - \frac{\bar{S}_s \bar{x}}{\bar{\mu}_s(\xi)} + \frac{-\xi + \bar{S}_0 - \bar{\beta}_s}{\bar{\mu}_0(\xi)} = 0. \quad (3.9)$$

We can show that the solution ξ_0, which is real and for which both $\bar{\mu}_s$ and $\bar{\mu}_0$ are real and positive, corresponds to the longshore wavenumber $l_0 = -R\gamma\xi_0$, which for a given frequency σ defines the group velocity path (or ray of energy flux) from the source point (x_0,y_0) in the outer ocean to the point (x,y) on the shelf.

This is shown schematically in Fig. 1. Here we have superimposed wavenumber space (k is the wavenumber in x) onto real space with the center of the dispersion circle for the T-R wave for a given frequency coinciding with the source point. We can do this because the angle θ is the same in each space. Part of the dispersion circle representing the shelf is drawn in the same (k,l) space as was done in I from which we can obtain the group velocity direction in real space for on the shelf. Thus, for a given point (x,y) on the shelf, a point of forcing (x_0,y_0) off the shelf and a frequency σ, the wavenumber l_0 will define the ray going from (x_0,y_0) to (x,y). Hence for one given frequency and the whole spectrum of wavenumbers which the delta functions will produce, the observed energy of the motion at a particular point on the shelf will be centered at the wavenumber l_0.

On the other hand, since we are more interested in frequency spectra, let us conceive of a point source of forcing with one dominant wavenumber and the whole spectrum of frequencies. In this case for given values of (x,y) and (x_0,y_0) we have a given value of l_0 from which we must calculate the frequency defining the ray. In Fig. 2 we show schematically the resulting rays for four different frequencies with a fixed wavenumber. In wavenumber space the dispersion circle decreases in radius and its center moves closer to the origin as frequency increases. Therefore, we have to superimpose the four wavenumber coordinates as shown with l_0 measured with respect to each.

We conclude from this figure that at a given point on the shelf there is one frequency σ_m of all the frequencies of waves produced at which the energy will be a maximum. This frequency is the one associated with l_0 producing the ray that goes to the point. If we move toward shore, say, on line A, σ_m will increase. If we move along shore in the positive y direction, say, on the line B, σ_m will also increase. Thus, we would expect to find an energy peak in the frequency spectrum at a frequency which depends on location.

Of course, (3.9) has other solutions also. A complex solution may be important in the vicinity of the shelf break (x near 0). In fact, for a given frequency, we can show that this complex solution becomes real for $x = 0$ if, in terms of dimensional quantities,

$$(y - y_0) \leqslant y_c - y_0 = \frac{-x_0[2l_c + \sigma^{-1}(f_0 S_0 - \beta_s)]}{2\mu_0(l_c)},$$

where $l_c = -R\gamma\xi_s = -S_s/4R$ is the critical wavenumber where $\mu_s = 0$. No wavenumber greater than l_c gets onto the shelf.

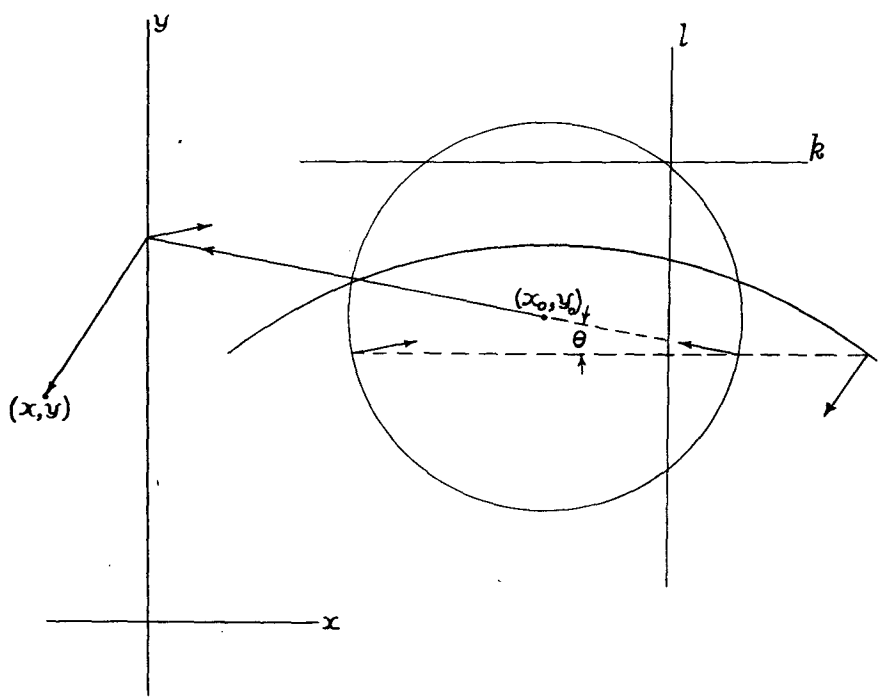

FIG. 1. Wavenumber space (k,l) superimposed on real space (x,y) as explained in the text.

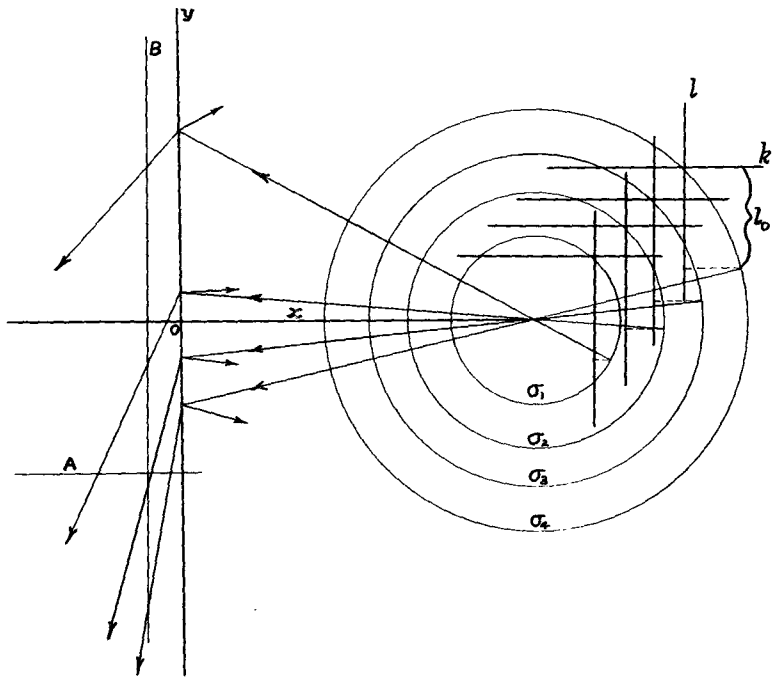

FIG. 2. Dispersion circles for various frequencies $\sigma_1 > \sigma_2 > \sigma_3 > \sigma_4$ in wavenumber space superimposed onto real space as explained in the text.

This is illustrated in Fig. 3. We see that it is possible for two different rays to go to a point on the shelf break. Even if the point is up the slope somewhat, the ray denoted by 2 in Fig. 3 may have a significant effect if the point is sufficiently close to the break. The ray denoted by 1 is the limiting ray from the solution $\xi_0 = \xi_s$ to (3.9) corresponding to the wavenumber l_c. It follows the break for $y - y_0 \leq y_c - y_0$.

We will use some of the qualitative notions in this section to interpret results from the application of realistic forcing which follows.

4. The solution for realistic forcing

Welch (1972) used an equation of the form

$$\tau = \frac{R_s^2 C_D}{\rho_a f^2} |\nabla p| (\mathbf{k} \times \nabla p \cos\lambda - \nabla p \sin\lambda) \quad (4.1)$$

to relate the surface wind stress to the surface variation of atmospheric pressure, where ρ_a is the air density, C_D the drag coefficient, R_s the shrinking constant and λ the veering angle. We want to describe the pressure field in a realistic manner, while at the same time obtaining a mathematically convenient wind stress curl. One such isolated pressure field is in terms of the incomplete gamma function

$$p = p_0 \frac{\Gamma(\tfrac{3}{4}, r'^2)}{\Gamma(\tfrac{3}{4}, 0)} = \frac{2p_0}{\Gamma(\tfrac{3}{4})} \int_{r'}^{\infty} t^{1/2} e^{-t^2} dt, \quad (4.2)$$

where p_0 is the maximum pressure difference at the center, $r' = r/L$ and $r = [(x - x')^2 + y^2]^{1/2}$. The field is centered at $(x',0)$ and the length L will be the measure of the radial scale of the pressure field.

Assuming f is constant, the wind stress curl resulting from this pressure field is given by

$$\tau' = \mathbf{k} \cdot \nabla \times \boldsymbol{\tau} = \tau_0' [1 - 2r'^2] e^{-2r'^2}, \quad (4.3)$$

where the maximum curl at $r' = 0$ is

$$\tau_0' = \frac{-8 R_s^2 C_D p_0^2 \cos\lambda}{\rho_a f_0^2 L^3 \Gamma^2(3/4)}.$$

For the purpose of calculation, we let $\tau_0' = \tau_{0N}' L_N^3 / L^3$, where τ_{0N}' is a nominal value of the maximum curl for a nominal scale of the pressure L_N. Welch noted that the maximum curl that he calculated from pressure data was rarely greater than 5×10^{-8} dyn cm^{-3}. So we choose this value for our nominal curl maximum and choose $L_N = 500$ km for the nominal scale. Fig. 4 shows the distribution of p/p_0 and τ'/τ_0' with r'. The curl in terms of dimensional quantities is

$$\tau' = \tau_{0N}' \frac{L_N^3}{L^3} (1 - 2r^2/L^2) e^{-2r^2/L^2}. \quad (4.4)$$

The streamfunction on the shelf for this forcing off the shelf is

$$\psi_s(x,y,t) = \int_0^{\infty} dx_0 \int_{-\infty}^{\infty} dy_0 \tau'(x_0,y_0) \psi_{sp}(x,y,t,x_0,y_0), \quad (4.5)$$

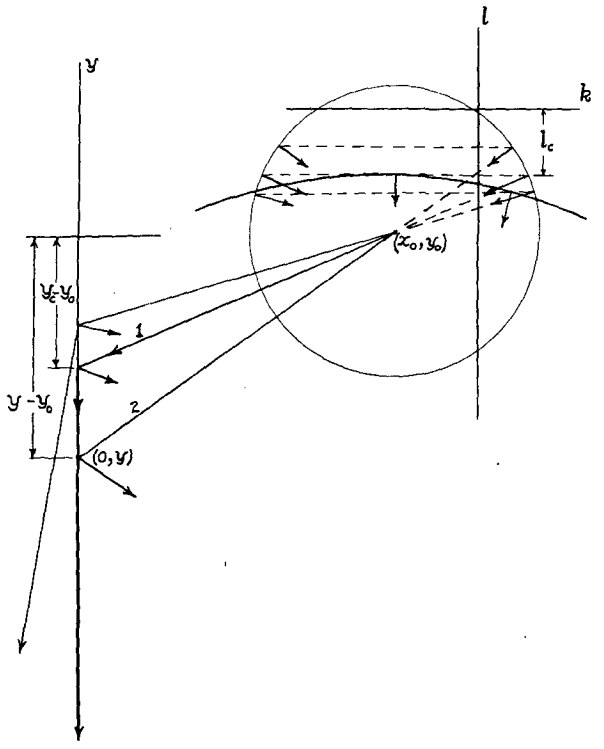

FIG. 3. Illustration that a point on the shelf break $(0,y)$ can have two different rays to it—one direct and the other along the break. l_c and y_c are defined in the text.

where ψ_{sp} is the point source solution (3.5) in dimensional variables and τ' is the curl from (4.4). Assuming that we can change the order of integration, Eq. (4.5) becomes in terms of dimensionless variables

$$\psi_s = \Psi_0 e^{-i\sigma t} \exp\left[\alpha\bar{x}\left(\frac{\bar{S}_s}{R} - i\bar{\beta}_c\right)\right] \exp\left[\alpha\left(i\bar{\beta}_c - \frac{S_0}{R}\right)\right]$$
$$\times \int_{-\infty}^{\infty} \frac{d\xi \exp[-i\alpha(\xi\bar{y} - \bar{\mu}_s\bar{x} + \bar{\mu}_0)]}{(\bar{S}_s - \bar{S}_0)/R + i(\bar{\mu}_s - \bar{\mu}_0)}$$
$$\times \int_{-x'/L}^{\infty} d\hat{x} \exp\left[\hat{\alpha}\left(i\bar{\beta}_c - \frac{S_0}{R} - i\mu_0\right)\hat{x} - 2\hat{x}^2\right]$$
$$\times \int_{-\infty}^{\infty} d\hat{y}[1 - 2(\hat{x}^2 + \hat{y}^2)] \exp(-2\hat{y}^2 + i\hat{\alpha}\xi\hat{y}), \tag{4.6}$$

where $\Psi_0 = (i/2\pi\sigma)\tau'_N(L_N^3/L)$, $\hat{x} = (x_0 - x')/L = (x'/L)(\bar{x}_0 - 1)$, $\hat{y} = y_0/L = (x'/L)\bar{y}_0$ and $\hat{\alpha} = \alpha L/x' = R\gamma L$.

The integral over $\hat{y}$ is a tabulated Fourier cosine integral. The subsequent integral over $\hat{x}$ can also be found exactly, but a much simpler form can be found if we assume that the forcing is sufficiently concentrated and its center is sufficiently far from the shelf break that the lower limit can be assumed to be essentially $-\infty$. Based on the assumption that

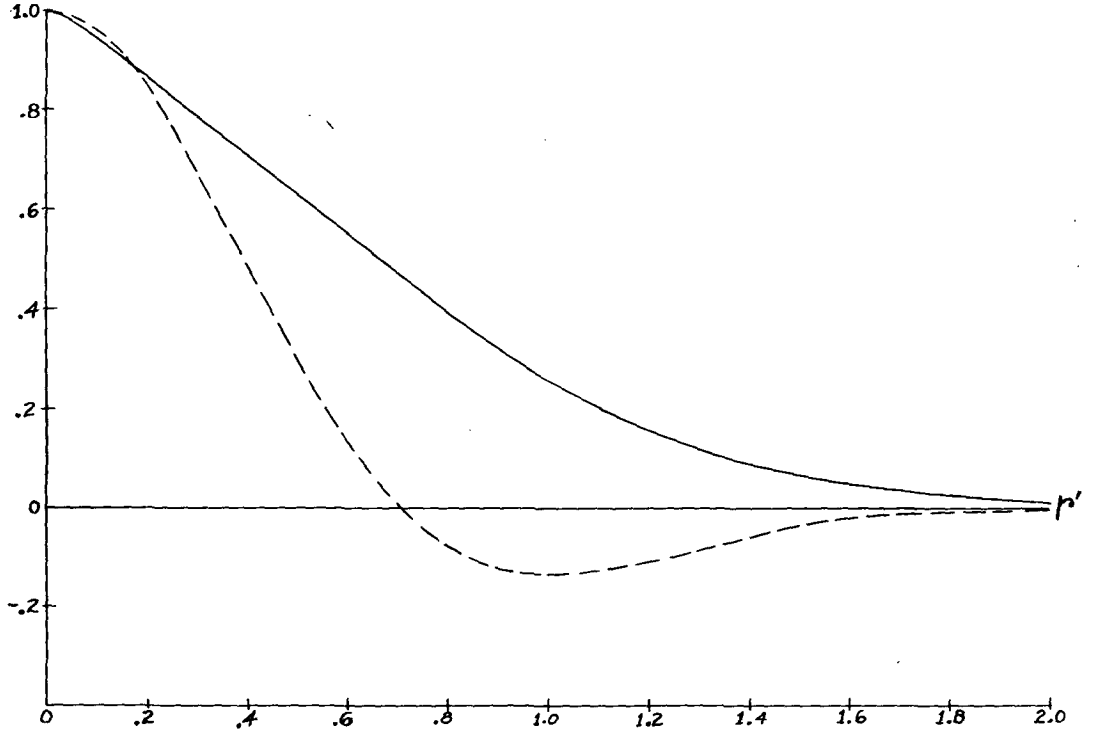

FIG. 4. The magnitude of p/p_0 (solid line) and τ/τ_0 (dashed line) plotted versus the dimensionless radius r'.

the integrand associated with the integration over ξ has essentially vanished for ξ such that $\hat{\alpha}[-\bar{\mu}_0^2(\xi)]^{1/2} \geq 5$ and that the complementary error function, $\operatorname{erfc}(z)$, has essentially vanished for $\operatorname{Re}[(z)^2] \geq 3$, we can show that this approximation varies only slightly in comparison with the exact integral if

$$\frac{x'}{L} \geq \frac{\hat{\alpha}\bar{S}_0}{4R} + \frac{5}{4} + \left[\frac{3}{2} + \left(\frac{\hat{\alpha}\bar{\beta}_c}{4}\right)^2\right]^{1/2}.$$

For realistic parameters $\hat{\alpha}\bar{S}_0/R$ and $\hat{\alpha}\bar{\beta}_c$ are small, thus this condition is approximately $x'/L \geq 2.5$.

We desire to calculate the kinetic energy which in this case means finding the longshore velocity component v since the magnitude of the cross-slope component $|u|$ is such that $|u|^2/|v|^2 \approx \xi_0/2\bar{S}_s \ll 1$ and hence is negligible for large period and wavelength waves. Using

$$v = \frac{\psi_{sx}}{H_0 e^{S_s x}} = \frac{\exp[(-2\bar{S}_s/R)\bar{x}]}{x' H_0}\,\psi_{s\bar{x}}$$

and integrating (4.6) twice, we find

$$v = V_0 e^{-i\sigma t}\exp[\alpha(i\bar{\beta}_c - \bar{S}_0/R)]\exp[-\alpha\bar{x}(\bar{S}_s/R + i\bar{\beta}_c)] \times \int_{-\infty}^{\infty} A(\xi)(q^2 + \xi^2)\exp[(-\hat{\alpha}^2/8)(q^2 + \xi^2)] \times \exp[-i\alpha(\xi\bar{y} - \bar{\mu}_s\bar{x} + \bar{\mu}_c)]d\xi, \quad (4.9)$$

where

$$A(\xi) = (\bar{S}_s - iR\bar{\beta}_c + iR\bar{\mu}_s)/[\bar{S}_s - \bar{S}_0 + iR(\bar{\mu}_s - \bar{\mu}_0)],$$

$$q = \bar{\beta}_c - \bar{\mu}_0(\xi) + i\bar{S}_0/R,$$

$$V_0 = \Psi_0 \frac{\pi\hat{\alpha}^2}{16}\frac{\alpha}{H_0 x'} = \frac{i}{32}\frac{\tau_N'}{H_0 f_0} L_N^3 L R^4 \gamma^3.$$

If $\bar{S}_s \gg \bar{S}_0$, $R\bar{\beta}_c$ implying $\bar{\mu}_s \gg \bar{\mu}_0$, $A(\xi)$ is approximately 1 except when $\xi \to \xi_s$ ($l \to l_c$). Evaluating q^2 in the exponential, an equivalent form of (4.9) is

$$v = V_0 e^{-i\sigma t}\exp[\alpha(i\bar{\beta}_c - \bar{S}_0/R)]\exp[-\alpha\bar{x}(\bar{S}_s/R + i\bar{\beta}_c)] \times \exp\left[-\frac{\hat{\alpha}^2}{4}\left(\bar{\beta}_c^2 - \frac{\bar{S}_0^2}{R^2} + i\frac{\bar{S}_0}{R}\bar{\beta}_c\right)\right] \times \int_{-\infty}^{\infty}\exp[-i\alpha(\xi y^* - \bar{\mu}_s\bar{x} + \bar{\mu}_0 x^*)] \times A(\xi)(q^2 + \xi^2)d\xi, \quad (4.10)$$

where

$$y^* = \bar{y} - \frac{i\hat{\alpha}^2}{4\alpha}(\bar{S}_0 - \bar{\beta}_s),$$

$$x^* = 1 - \frac{\hat{\alpha}^2}{4\alpha}\left(\frac{\bar{S}_0}{R} - i\bar{\beta}_c\right).$$

It would be nice if we could evaluate the integral of (4.9) using asymptotic techniques, but the parameter α[$\leq O(10)$ realistically] would not seem to be sufficiently large to do this accurately. Thus numerical means must be employed for an accurate solution. However, we will still employ the saddle-point method assuming that the parameter α is large. We will see that the asymptotic result will compare poorly with the numerical result for the amplitude of v but fairly well in finding frequency maxima. We interpret this to mean that the functional character of the asymptotic solution is a better approximation than its amplitude and is therefore useful in deriving some general results with greatly less effort than numerical integration.

The form (4.10) is used for the numerical integration. To lessen the effect of rapid oscillations, a path of steepest descent through a saddle point should be used. However, the numerical calculation of this path is not economical. A compromise path, where the $i\alpha\bar{\mu}_s\bar{x}$ term is excluded from the eiconal determining the saddle point and path, and a Gaussian quadrature routine using many points is much more economical.

It would be best to use the form (4.10) also for the asymptotic solution. But if the forcing is sufficiently concentrated, we can use only that part of the eiconal of (4.9) which is like that of the integral for the point source (3.5) and assume the rest of the integrand varies slowly in comparison.

Thus we define the phase function

$$E(\xi) = -i[\xi\bar{y} - \bar{\mu}_s(\xi)\bar{x} + \bar{\mu}_0(\xi)] \quad (4.11)$$

and let

$$F(\xi) = A(\xi)[q^2(\xi) + \xi^2]\exp[(-\hat{\alpha}^2/8)(q^2 + \xi^2)], \quad (4.12)$$

where we assume F changes slowly compared to $e^{\alpha E(\xi)}$. The integral of (4.9) is then of the form

$$I = \int_{-\infty}^{\infty} F(\xi)e^{\alpha E(\xi)}d\xi. \quad (4.13)$$

Setting $E'(\xi) = 0$ we find the equation for the saddle points is the same as (3.9) for the point source if $y - y_0$ is replaced by $\bar{y}$:

$$\bar{y} + \frac{-\frac{1}{2}(2\bar{S}_s)^{1/2}\bar{x}}{(\xi - \xi_s)^{1/2}} + \frac{-\xi + (\bar{S}_0 - \bar{\beta}_s)}{[(\xi_{0+} - \xi)(\xi - \xi_{0-})]^{1/2}} = 0, \quad (4.14)$$

where $\xi_{0\pm} \approx \bar{S}_0 - \bar{\beta}_s \pm 1$ and $\xi_s \approx \bar{S}_s/2R^2$. A comparison of (4.14) with the similar equation developed using the whole eiconal part of (4.10) shows that for the worst case where $\bar{x} = \bar{y} = 0$, we must have $\hat{\alpha}^2/4\alpha \ll 1$ (or $L^2 \ll 4x'/R\gamma$) to be able to use (4.11) rather than the whole eiconal of (4.10).

The integral (4.13) has the same branch points and cuts as (3.5) and similarly has no poles. As with the point source it can be shown that besides the primary root ξ_0, where $\xi_s < \xi_0 < \xi_{0+}$, corresponding to ξ_0 for (3.9), there is a secondary root which

is complex below (except at $\bar{x} = 0$) and real above a certain curve that begins at $\bar{x} = 0, \bar{y} = \bar{y}_c = (\xi_s - \bar{S}_0 + \bar{\beta}_c)/\bar{\mu}_0(\xi_s)$ going to $\bar{x} \to -\infty, \bar{y} \to -\infty$. The branch from ξ_s must lie to the right of this root for this root to exist.

Remembering that $\xi_{0-} < \xi_s < \xi_{0+}$, $0 < \xi_s = S_s/2R^2$ and noting that $\xi_{0+} - \xi_0 = 2$, we consider two extreme cases. The first case is $\xi_{0+} = 2$ and $\xi_{0-} = 0$ which means for $0 < \xi_s < 2$, corresponding to $(\bar{S}_s)^{1/2}/2 < R < \infty$, we have waves onto the shelf. This is the case where the "window" onto the shelf is fully open. The second case is $\xi_{0+} = 0$ and $\xi_{0-} = -2$ which means there are no waves at any R onto the shelf. The window is closed. The first case is approached for $S_0 - \beta_s/f_0 \gg |\beta_c/f_0|$, the second for $\beta_s/f_0 \gg S_0$, $|\beta_c/f_0|$, which can be true only for x directed to the north. The halfway case is $\xi_{0+} = 1$ and $\xi_{0-} = -1$ which means $0 < \xi_s < 1$ corresponding to $(\bar{S}_s/2)^{1/2} < R < \infty$. This third case is approached for $|\beta_c/f_0| \gg |S_0 - \beta_s/f_0|$ and can only occur for x directed mainly east or west.

It can be shown that the secondary root is not important for $|\bar{y}| = O(1)$ in the contour integration of (4.13) for the first case and a fairly simple approximation can be found. This is not true for the other cases. Fortunately, the first case is quite realistic since small topographic changes dominate the beta effect. So we will consider $S_0 - \beta_s/f_0 \gg |\beta_c/f_0|$ from now on but not totally neglect the beta effect.

We then want to integrate over a path of steepest descent through the saddle point ξ_0. This path will be the locus of all points $z = \xi + i\eta$ such that from (4.11)

$$E(z) - E(\xi_0) = -u^2, \tag{4.15}$$

where u is always real. Using contour integration around a closed contour we can show that (4.13) becomes

$$I = -2e^{\alpha E(\xi_0)} \int_{-\infty}^{\infty} H(u) e^{-\alpha^2 u^2} du, \tag{4.16}$$

where $H(u) = uF[z(u)]/E'[z(u)]$. Then expanding $H(u)$ in a Maclaurin series and integrating (4.16) term by term, we obtain

$$I = -2e^{\alpha E(\xi_0)} H(0) \sqrt{\frac{\pi}{\alpha}} \left[1 + \frac{H''(0)}{4\alpha H(0)} + \cdots \right], \tag{4.17}$$

where we calculate $H(0) = F(\xi_0)/[-2E''(\xi_0)]^{1/2}$, the proper branch of the radical determined by the path (4.15) for $z \to \xi_0$. $H''(0)$ and higher derivatives are considerably more complicated and not reproduced here because we will use only the lowest order approximation.

The lowest order approximation of I is then

$$I \approx -2\left(\frac{\pi}{\alpha}\right)^{1/2} \frac{e^{\alpha E(\xi_0)}}{(2\rho)^{1/2}} A(\xi_0) Q(\xi_0) \times \exp[-(\hat{\alpha}^2/8) Q(\xi_0)] e^{i(\pi/4)}, \tag{4.18}$$

where

$$Q(\xi_0) = q^2(\xi_0) + \xi_0^2,$$

$$\rho(\xi_0) = \frac{-\bar{x}}{4} (2\bar{S}_s)^{1/2} (\xi_0 - \xi_s)^{-3/2} + \frac{(\bar{S}_0 - \bar{\beta}_s - \xi_0)^2}{[(\xi_0 - \xi_{0+})(\xi_{0-} - \xi_0)]^{3/2}} + \frac{1}{[(\xi_0 - \xi_{0+})(\xi_{0-} - \xi_0)]^{1/2}}.$$

Then the square of the velocity amplitude from (4.9), evaluating α and $\hat{\alpha}$ to show the dependence on R, is given by

$$|v|^2 \approx \frac{2\pi}{(32)^2} \frac{\tau_N'^2 L_N^6 L^2 \gamma^5}{H_0^2 f_0^2 x' \rho(\xi_0)} \exp(-2\gamma \bar{S}_s x - 2\gamma \bar{S}_0 x') \times |Q(\xi_0)|^2 R^7 \exp(-\gamma^2 L^2 Q' R^2/4), \tag{4.19}$$

where $Q' = \mathrm{Re}\{Q\} = \xi_0^2 + (\bar{\beta}_c - \bar{\mu}_0)^2$. To find ξ_0 we must numerically solve (4.14). If R_m, the value of R at which $|v|^2$ is a maximum, is sufficiently large such that $\xi_0 \gg \xi_s = \bar{S}_s/2R_m^2$, the solution ξ_0 of (4.14) will be essentially independent of R_m and so will $\rho(\xi_0)$.

The value for R which maximizes $|v|^2$ can then be found from (4.19) assuming ξ_0 and ρ are essentially independent of R. We thus obtain

$$R_m = \frac{f_0}{\sigma_m} \approx \frac{\sqrt{14}}{\gamma L \sqrt{Q'}}, \tag{4.20}$$

where Q' is defined after (4.19). In comparison with the more accurate numerical integration we will find that (4.20) is much better than (4.19). σ_m will be the dominant frequency at a given point on the shelf. It is the frequency at which $|v|^2$ is a maximum for given values of x, y, x' and L. The wavenumber $l_m = -R_m \gamma \xi_0$, where ξ_0 is evaluated from (4.14) for the given values of x, y, and x' will be the dominant wavenumber at that given point on the shelf. The dominant wavelength is defined by $\lambda_m = 2\pi/|l_m|$.

The easiest way to estimate the frequency of the energy peak which might be expected on a given shelf is to let $\bar{x}$ and $\bar{y}$ vanish, implying $\xi_0 = \bar{S}_0 - \bar{\beta}_s$ and so $Q = 2(1 - \bar{\beta}_c)$, and use (4.20) to obtain

$$\frac{\sigma_m}{f_0} = \frac{1}{R_m} \approx \frac{\gamma L (1 - \bar{\beta}_c)^{1/2}}{\sqrt{7}}. \tag{4.21a}$$

An estimate of the associated wavelength is then

$$\lambda_m = \frac{2\pi}{|l_m|} = \frac{2\pi L (1 - \bar{\beta}_c)^{1/2}}{\sqrt{7}(\bar{S}_0 - \bar{\beta}_s)}. \tag{4.21b}$$

In the Northern Hemisphere since $\bar{\beta}_c > 0$ for an east coast shelf and $\bar{\beta}_c < 0$ for a west coast shelf, we would expect a lower frequency on the former.

We must remember that (4.20) and (4.21) are valid only for $S_0 - \beta_s/f_0 \gg |\beta_c/f_0|$, which implies $1 \gg |\bar{\beta}_c|$, and for $\xi_0 \gg \bar{S}_s/2R_m^2$. The comparison with numerical results, however, shows that (4.20) is quite accurate for $|\bar{\beta}_c|$ approaching 0.4 and $\bar{S}_s/2R_m^2\xi_0$ approaching 0.33. So there is some latitude in these conditions.

5. Numerical results and comparison with data

We will apply the model to the Oregon shelf at 45°N assuming the following values for the associated parameters: $S_0 = 0.35 \times 10^{-8}$ cm^{-1}, $S_s = 0.3 \times 10^{-6}$ cm^{-1}, $\beta_c = -1.3 \times 10^{-13}$ cm^{-1} s^{-1}, $\beta_s = 0$, $f_0 = 1.03 \times 10^{-4}$ s^{-1}, $H_0 = 2.4 \times 10^5$ cm. The parameters associated with the forcing are $\tau_N' = 5 \times 10^{-8}$ dyn cm^{-3} and $L_N = 500$ km.

Results using numerical integration are shown on Fig. 5. Here the square of the longshore velocity $|v|^2$ at a particular point on the shelf is plotted versus frequency. In this case the pressure cell has a scale $L = L_N$ and is centered a distance (x') 2000 km west of the shelf break. The location on the shelf with respect to our coordinate system is $y = -2000$ km (2000 km north of the center of forcing) and $x = -106$ km corresponding to the 100 m isobath.

This figure is typical for any location on the shelf with $|v|^2$ having a single maximum at some frequency σ_m, $|u|^2$ will also have a maximum at σ_m but will be over two orders of magnitude less than $|v|^2$. That $|v|^2$ has a maximum is consistent with our notions in Section 3. From Fig. 5 we see that the energy $|v|^2$ peaks at around $\sigma_m = 0.05$ cpd. The data of Smith (1974), from a 48-day record from current meters over the 100 m isobath off Oregon, show a definite peak around this frequency. Since the record is 48 days and the peak has a period of 20 days, there is a question about its statistical significance. However, it would seem to be possible that the peak is real.

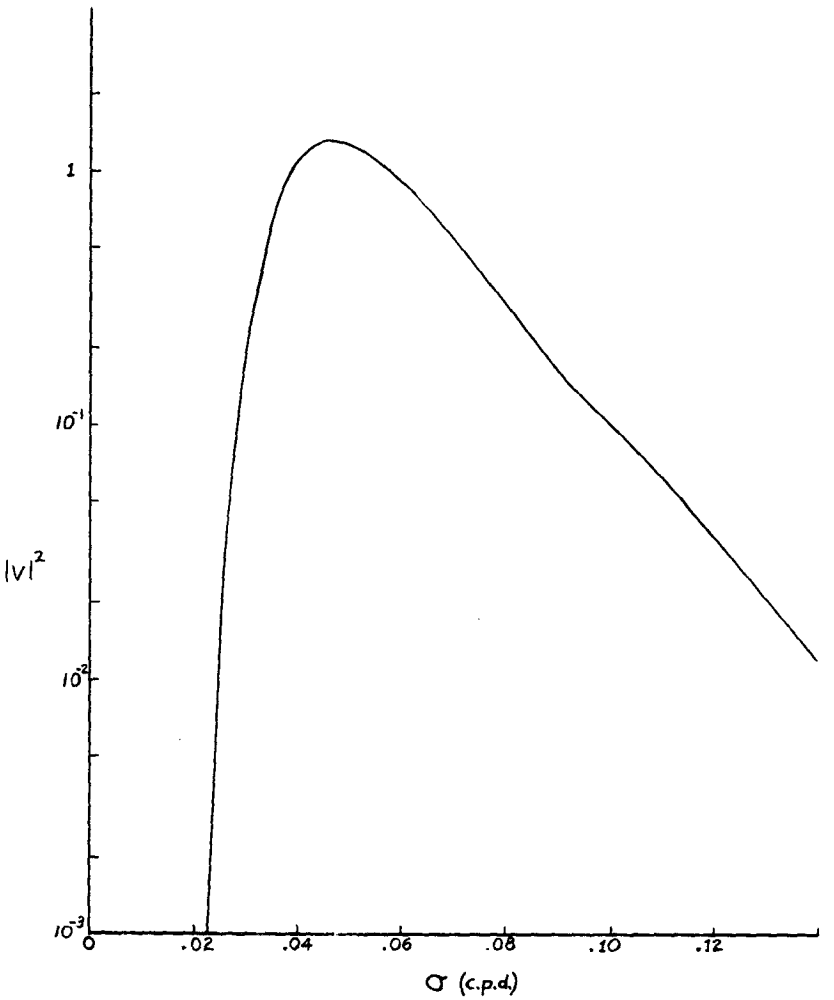

FIG. 5. Numerical calculations of the square of the amplitude of the longshore velocity $|v|^2$ (cm^2 s^{-2}), as a function of the frequency σ (cpd) for $y = -2000$ km, $x' = 2000$ km, $L = 500$ km and $h = 100$ m.

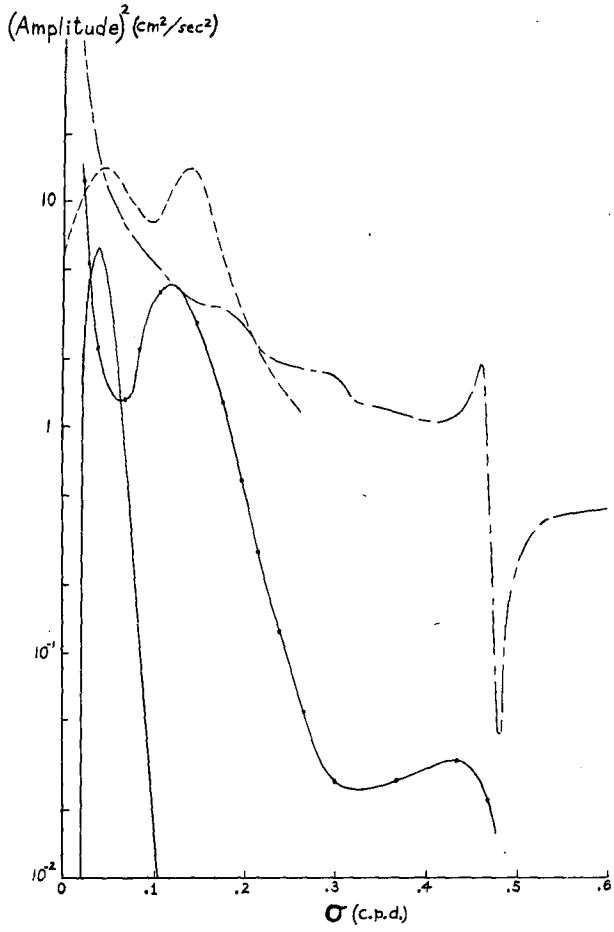

FIG. 6. $|v|^2$ from the numerical calculations for off the shelf (solid line) and on the shelf [(long dashes) for a flat wind spectrum, (dotted line) for a local wind spectrum] compared to the data of Smith (short dashes). The parameters are given in the text.

Fig. 6 shows the energy data, the calculated energy produced by a pressure cell off the shelf, and the calculated energy produced by a longshore wind on the shelf. The model describing the motion on the shelf is similar to that of Adams and Buchwald (1969). This model, of course, has a shore boundary. We assume that the wind stress is uniform across the 120 km wide shelf and decays exponentially in opposite directions along shore from $y = 0$. The calculation consists of adding shelf modes which, for frequencies of the order of 0.05 cpd, necessitates adding up to 50 modes. The magnitude of the wind stress used is 0.3 (cm s^{-1})^2 which is the same as the maximum stress associated with the magnitude of the curl used off the shelf. The e-folding length of the forcing along the shelf is the same as L, 500 km.

The forcing on the shelf is included to show that it does not have a peak near 0.05 cpd. We show this calculation for the stress independent of frequency and also with the frequency variation of the wind spectrum data from Smith. The peak at 0.14 cpd correlates strongly with the wind, but the peak at 0.05 cpd does not. The addition of the energy from off the shelf with that from on the shelf would give us the double peak observed in the data. In choosing $x' = 500$ km the energy from off the shelf seems to have a realistic magnitude.

6. Properties of results and discussion

We now examine the properties of the energy generated off the shelf, concentrating on $|v|^2$. We use the parameters for the Oregon shelf to investigate the variation of the maximum energy $|v_m|^2$ and the frequency σ_m of that maximum with the loca-

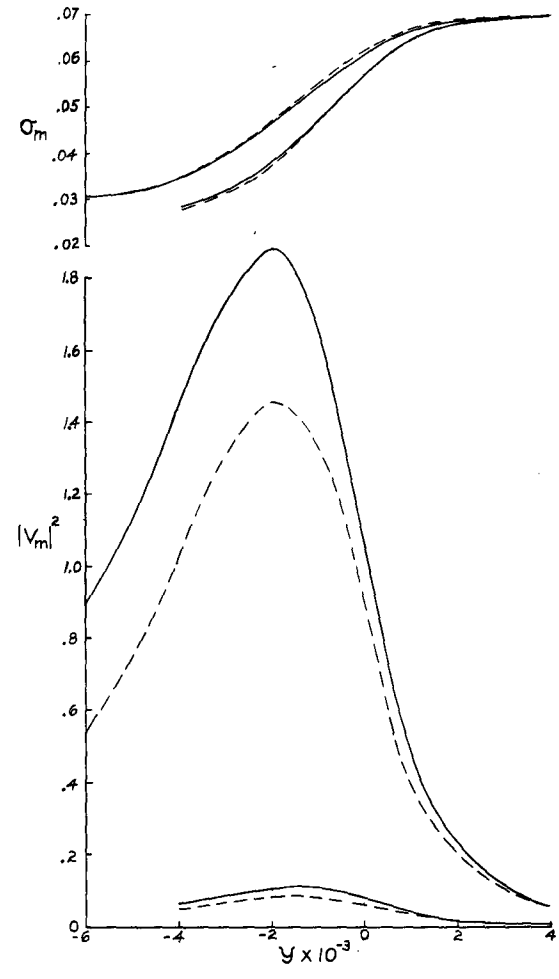

FIG. 7. The maximum amplitude squared $|v_m|^2$ (cm^2 s^{-2}) and the frequency of the maximum σ_m (cpd) versus the longshore location y (km). The solid line is the numerical integration and the dashed is the saddle-point calculation. The higher pair of curves in each plot is for $h = 100$ m, while the lower pair is for the shelf break ($h = 2400$ m). $x' = 2000$ km, and $L = 500$ km.

tion on the shelf (x,y), the distance of the center of forcing from the shelf x' and the scale of forcing L. Also, the results from the numerical integration are compared to those of the saddle-point method, and the dominant wavelength λ_m associated with σ_m is calculated.

Fig. 7 shows $|v_m|^2$ and σ_m as functions of the longshore location y at the shelf break ($x = 0$) and the 100 m isobath ($x = -106$ km) for fixed values of $x' = 2000$ km and $L = 500$ km. We see that the energy is a maximum around $y = -2000$ km for $x = -106$ km and $y = -1000$ km for $x = 0$. The frequency behaves according to our notions in Section 3, increasing with increasing y. In other words, the frequency decreases as you move along shore with the shore on your right in the Northern Hemisphere.

Over a distance of 10 000 km along shore, the frequency changes from about 0.03 to 0.07 cpd. The value for σ_m given by (4.21a) is 0.057 cpd. In the cross-shelf direction the frequency increases toward shore, consistent with our notions in Section 3. However, the frequency change over the shelf width of O(100 km) is small, being negligible for y large and increasing to the order 0.01 cpd at $y = -2000$ km. As the center of forcing gets closer to the shelf, however, this difference should increase.

The comparison of the saddle-point calculation for $|v_m|^2$ with the numerically integrated result, which we consider accurate, is fair for $|v_m|^2$ and very good for σ_m for both $x = -106$ km and $x = 0$.

Fig. 8 shows the variation of $|v_m|^2$ and σ_m with the distance x' of the center of forcing from the shelf break. $|v_m|^2$ is plotted for $y = -2000$ km and σ_m for $y = -2000$, 0, 2000 km with the fixed parameters $L = 500$ km and $x = -106$ km. Of course, $|v_m|^2$ increases as the center of forcing nears the shelf. σ_m may increase ($y = -2000$ km) or decrease ($y = 0$, 2000 km) with x' depending on longshore location and somewhat less on the cross-shelf location. The saddle-point result for $|v_m|^2$ becomes poorer as the center of forcing approaches the shelf as expected. Again, however, the saddle-point result for σ_m compares much better.

The saddle-point method allows us to calculate the approximate dominate wavelength λ_m (or wavenumber l_m) associated with σ_m using Eq. (4.14). Fig. 9 shows both λ_m and l_m plotted versus σ_m for the forcing scale $L = 500$ km. This figure actually encompasses to a good approximation the variation of all the other parameters except L. What we see is the fact that this forcing cannot be considered to be characterized by one single wavelength, since λ_m varies with frequency. In fact, l_m is close

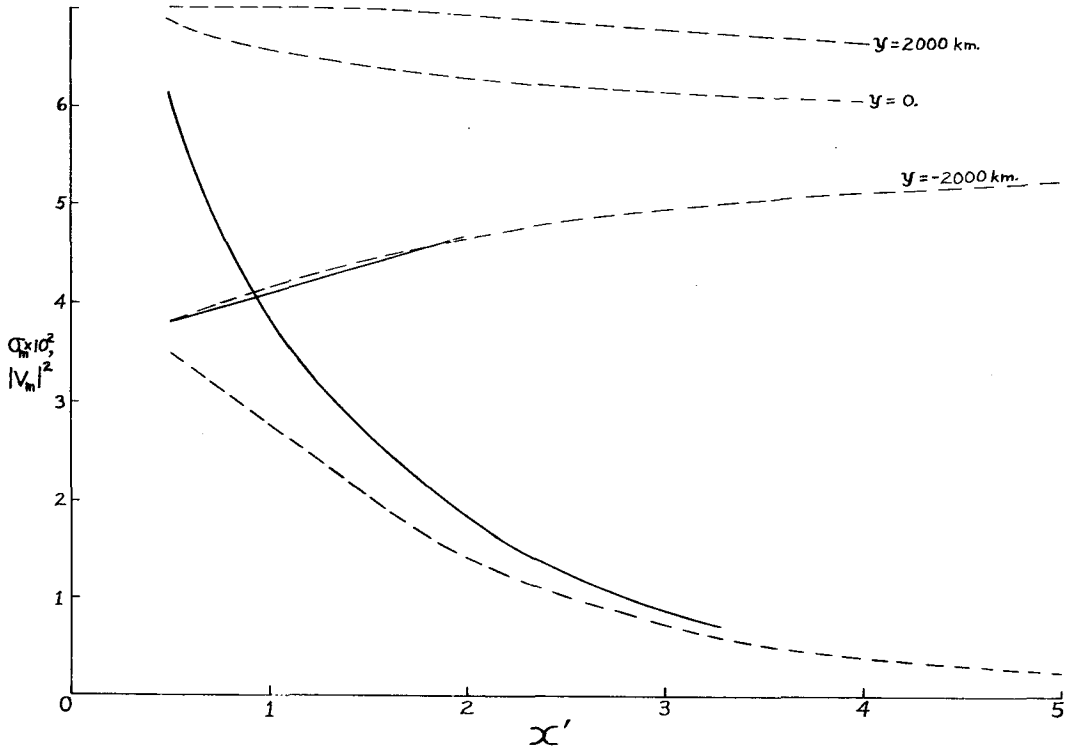

FIG. 8. $|v_m|^2$ (cm^2 s^{-2}) and σ_m (cpd) versus the location of the center of forcing x' (10^3 km). Solid curves represent numerical integration, dashed the saddle-point method. The bottom solid and dashed line are $|v_m|^2$ for $y = 2000$ km, $h = 100$ m and $L = 500$ km. The rest of curves are σ_m for various y and the same h and L.

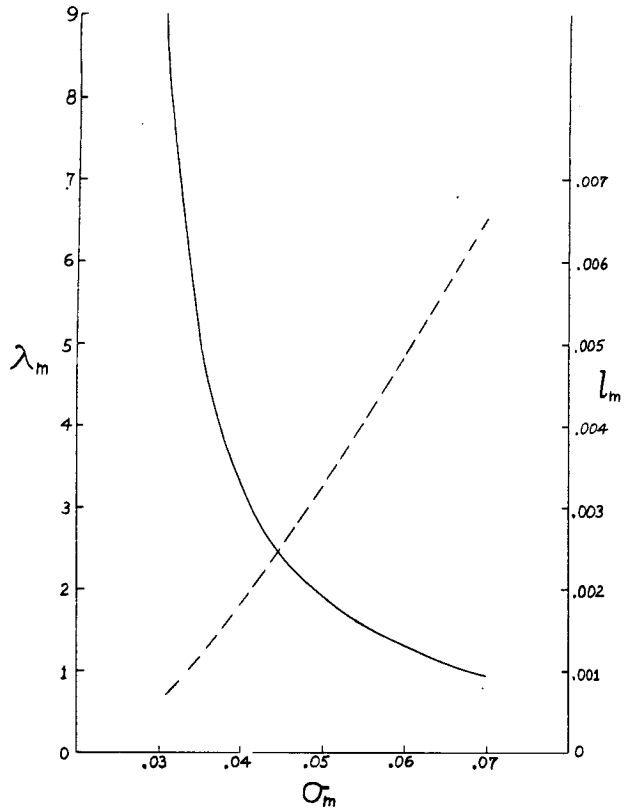

FIG. 9. The dominant wavelength λ_m (10^3 km, solid line) and wavenumber, l_m (km^{-1}, dashed line), versus σ_m (cpd) for L = 500 km.

to being a linear function of σ_m. Our notions in Section 3 were based on l_m not changing with σ_m, but the qualitative results are the same. Considering this figure in conjunction with Fig. 7, if we move along the shelf with the shore to our right, we would expect the dominant wavelength to increase, gradually at first for $y \geq 0$ and faster as y became more negative. For the observed peak at 0.05 cpd, the dominant wavelength should be about 2000 km for the parameters we used. The estimate given by Eq. (4.21b) is λ_m = 1450 km for σ_m = 0.057 cpd from Eq. (4.21a).

Fig. 10 shows the variation of $|v_m|$ and σ_m with the scale L of the pressure cell generating the stress curl with the fixed parameters $x = -106$ km, $y = -2000$ km and $x' = 2000$ km. The tremendous increase in $|v_m|$ as L decreases is due to the reciprocal cubic variation of τ' with L as seen in (4.3). This calculation represents holding the magnitude of the pressure difference constant while changing the scale of the pressure cell. This result illustrates that to accurately calculate the magnitude of the energy, the intensity and especially the scale of the pressure cell must be accurate.

The frequency σ_m increases approximately linearly with L. Fig. 9 cannot be used to find λ_m for these values of σ_m. In this case λ_m and σ_m are each approximately linear functions of L and hence with each other.

7. Conclusions

The low-frequency, long-wavelength energy generated by the wind stress curl off the shelf should appear as a distinct peak at low frequency in the energy spectrum on the shelf. All parameters being equal, the peak should have a lower frequency on an eastern shelf than a western shelf in the Northern Hemisphere due to the beta effect. For the Oregon shelf this peak should be between about 0.02 and 0.08 cpd, depending on the location on the shelf in relation to the center of forcing and on the scale of the forcing. The magnitude also depends on these parameters, especially the forcing scale. It is plausible that the peak at 0.05 cpd in the data of Smith (1974) is not spurious but due to the energy from off the shelf.

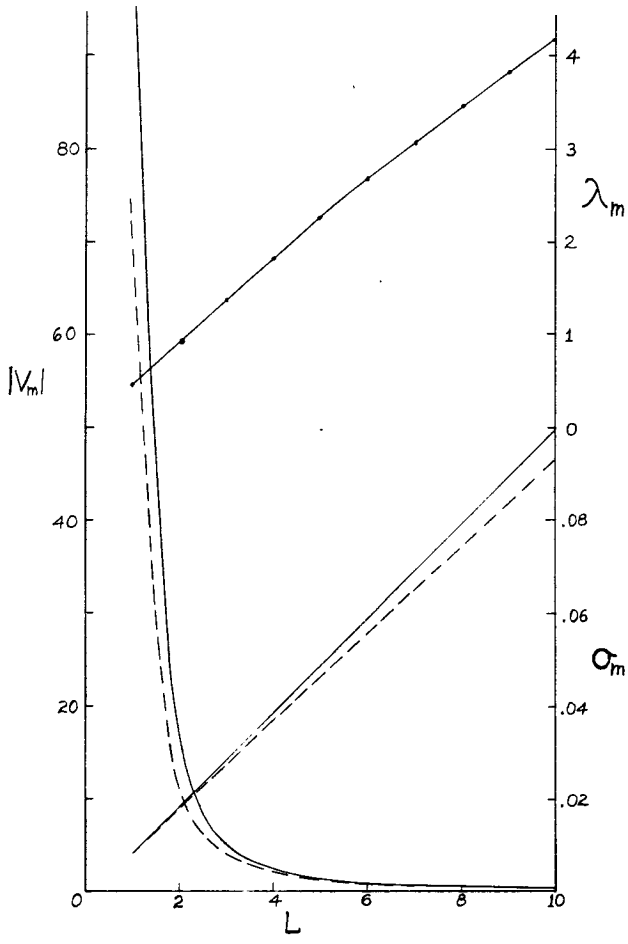

FIG. 10. Maximum amplitude $|v_m|$ (cm s^{-1}), dominant wavelength λ_m (10^3 km) and frequency of maximum σ_m (cpd) versus the scale of the forcing L (10^2 km) for $y = -2000$ km, h = 100 m and x' = 2000 km.

The quantitative results are open to question because of the oversimplified topography assumed. The topography off the shelf is especially critical, and our assumption that this slope is exponential and varies in only one direction is poor. For this reason it would not seem profitable to make more elaborate calculations using this model. Certainly, any refinement should consider the baroclinicity off the shelf. However, the estimate of the frequency and wavelength of the energy peak given by Eqs. (4.21a) and (4.21b) should still be useful approximations.

REFERENCES

Adams, J. K., and V. T. Buchwald, 1969: The generation of continental shelf waves. *J. Fluid Mech.*, **35**, 815–826.

Kroll, J., and P. P. Niiler, 1976: The transmission and decay of barotropic topographic Rossby waves incident on a continental shelf. *J. Phys. Oceanogr.*, **6**, 432–450.

Smith, R. L., 1974: A description of current, wind, and sea level variations during coastal upwelling off the Oregon coast, July–August 1972. *J. Geophys. Res.*, **79**, 435–443.

Welch, C. S., 1972: On the calculation of wind stress curl over open ocean areas from synoptic meteorological data with application to time-dependent ocean circulation. Unpublished manuscript, Ref. No. 72-6, Woods Hole Oceanographic Institution, 189 pp.